Langmuir
Article
pubs.acs.org/Langmuir

Frictional Forces between Strongly Compressed, Nonentangled Polymer Brushes: Molecular Dynamics Simulations and Scaling Theory

A. Galuschko,[†] L. Spirin,[‡] T. Kreer,*[,†] A. Johner,[†] C. Pastorino,[§] J. Wittmer,[†] and J. Baschnagel[†]

[†]*Institut Charles Sadron, 23 rue du Loess, BP 84047, 67034 Strasbourg Cedex 2, France,* [‡]*Institute of Physics, Johannes Gutenberg-University, Staudinger Weg 7, 55099 Mainz, Germany, and* [§]*Physics Department CAC−CNEA, Av. Gral. Paz 1499, Pcia. Buenos Aires (1650), Argentina*

Received October 29, 2009. Revised Manuscript Received December 17, 2009

By means of molecular dynamics simulations and scaling theory we study the response of opposing polymer brushes to constant shear motion under good solvent conditions. Model systems that contain explicit solvent molecules (Lennard-Jones dimers) are compared to solvent-free systems while varying of the distance between the grafted layers and their molecular parameters, chain length and grafting density. Our study reveals a power-law dependence of macroscopic transport properties on the Weissenberg number, W, beyond linear response. For instance, we find that the kinetic friction constant scales as $\mu \sim W^{0.57}$ for large values of W. We develop a scaling theory that describes our data and previous numerical data including recent experiments.

I. Introduction

Polymers adsorbed on surfaces are important in many phenomena and applications, such as adhesion,[1] stabilization of colloidal dispersions,[2] protection against corrosion,[3] flotation of minerals,[4] oil recovery,[5] smart materials,[6] wetting and spreading phenomena,[7,8] biotechnology,[9] and so forth. Of specific interest are polymers that are grafted onto a surface by one chain end, so-called "polymer brushes".[7] In a polymer brush, chains tend to stretch away perpendicular from the substrate due to the steric repulsion between the monomers. Opposing brush-covered surfaces can carry very high normal loads, whereas simultaneously the resistance to lateral sliding motion can be extremely small. The resulting friction coefficients may be orders of magnitude smaller than those found in dry friction.[10,11] Polymer brushes have thus important applications as lubricants, e.g., in machine parts or artificial joints.[9] Moreover, they are believed to play a crucial role in biolubrication, e.g., in synovial joints.[12]

While the extremely low friction forces between polymer brushes are well established experimentally (see, e.g., refs 10−13), the understanding of the underlying mechanism is still rather incomplete. This difficulty is mainly related to the fact that, in experiments, it is almost impossible to provide sufficiently detailed information about the molecular factors causing the rheological response of the grafted layers to external stimuli. In this respect, computer simulations provide a promising avenue because the simulation can be employed as a "high-resolution microscope" to explore structure−property relations of studied (model) systems. This may account for much of the large activity in this field over the past few decades (see, e.g., refs 13−31).

The vast majority of the numerical approaches have treated solvent effects without explicitly including solvent molecules in the simulation (implicit solvent simulation). For instance, in molecular dynamics (MD) simulations,[8,14,15,19,24,26,27,29,30] this has been done via the application of thermostats and the adjustment of the interaction potential between the monomers. Other approaches have been made[13,16,17,20,21] by solving the Brinkman equation[32] for solvent- and monomer-flow field self-consistently. Solvent effects as well can be considered implicitly via the lattice−Boltzmann method (see ref 33 and references therein) or

*Corresponding author.

(1) Brown, H. R. *IBM J. Res. Dev.* **1994**, *38*, 379. Druelle, M.; Leger, L. *Macromolecules* **1995**, *28*, 7419. Ligoure, C. *Macromolecules* **1996**, *29*, 5459.
(2) Gast, A.; Leibler, L. *Macromolecules* **1986**, *19*, 686. Borukhov, I.; Leibler, L. *Phys. Rev. E* **2000**, *62*, R41.
(3) Wootton, I. A.; Spainhour, L. K.; Yazdani, N. *Compos. Constr.* **2003**, *7*, 339.
(4) Pugh, R. J. *Int. J. Miner. Process.* **1989**, *25*, 101. Bogusz, E.; Brienne, S. R.; Butler, I.; Rao, S. R.; Finch, J. A. *Miner. Eng.* **1997**, *10*, 441. Boulton, A.; Fornasiero, D.; Ralston, J. *Int. J. Miner. Process.* **2001**, *61*, 13.
(5) Stanislav, J. F. *Rheol. Acta* **2005**, *21*, 564.
(6) Roy, I.; Gupta, M. N. *Chem. Bio.* **2003**, *10*, 1161.
(7) Advincula, R. C., Brittain, W. J., Caster, K. C., Rühe, J., Eds.; *Polymer Brushes*; Wiley-VCH: Weinheim, Germany, 2004.
(8) Müller, M.; Pastorino, C.; Kreer, T.; Binder, K.; Mac-Dowell, L. G. *ACS Abstr.* **2006**, *231*, 416-PMSE.
(9) Moro, T.; Takatori, Y.; Ishihara, K.; Konno, T.; Taki-gawa, Y.; Matsushita, T.; Chung, U.; Nakamura, K.; Kawaguchi, H. *Nat. Mater.* **2004**, *3*, 829.
(10) Klein, J.; Perahia, D.; Warburg, S. *Nature* **1991**, *352*, 143.
(11) Klein, J. *Annu. Rev. Mater. Sci.* **1996**, *26*, 581.
(12) Klein, J. *Proc. IMechE J.* **2006**, *220*, 691. Klein, J. *Science* **2009**, *323*, 47.
(13) Schorr, P. A.; Kwan, T. C. B.; Kilbey, S. M., II; Shaqfey, E. S. G.; Tirrell, M. *Macromolecules* **2003**, *36*, 389.
(14) Murat, M.; Grest, G. S. *Phys. Rev. Lett.* **1989**, *63*, 1074.
(15) Grest, G. S.; Murat, M. *Macromolecules* **1993**, *26*, 3108.
(16) Lai, P.-Y.; Binder, K. *J. Chem. Phys.* **1993**, *98*, 2366.
(17) Miao, L.; Hong, G.; Zuckermann, M. J. *Macromolecules* **1996**, *29*, 2289.
(18) Lai, P.-Y.; Lai, C.-Y. *Phys. Rev. E* **1996**, *54*, 6958.
(19) Grest, G. S. *Phys. Rev. Lett.* **1997**, *76*, 4979.
(20) Doyle, P. S.; Shaqfeh, E. S. G.; Gast, A. P. *Phys. Rev. Lett.* **1997**, *78*, 1182. *Macromolecules* **1998**, *31*, 5474.
(21) Saphiannikova, M. G.; Pryamitsyn, V. A.; Cosgrove, T. *Macromolecules* **1998**, *31*, 6662.
(22) Neelov, I. M.; Borisov, O. V.; Binder, K. *Macromol. Theory Simul.* **1998**, *7*, 141.
(23) Grest, G. S. In *Advances in Polymer Science*; Granick, S.,Eds; Springer: Berlin, 1999; Vol. *138*, p 149.
(24) Kreer, T.; Müser, M. H.; Binder, K.; Klein, J. *Langmuir* **2001**, *17*, 7804.
(25) Irfachsyad, D.; Tildesley, D.; Malfreyt, P. *Phys. Chem. Chem. Phys.* **2002**, *4*, 3008.
(26) Kreer, T.; Binder, K.; Müser, M. H. *Langmuir* **2003**, *19*, 7551.
(27) Kreer, T.; Müser, M. H. *Wear* **2003**, *254*, 827.
(28) Goujon, F.; Malfreyt, P.; Tildesley, D. J. *ChemPhysChem* **2004**, *5*, 457. *Mol. Phys.* **2005**, *103*, 2675.
(29) Pastorino, C.; Binder, K.; Kreer, T.; Müller, M. *J. Chem. Phys.* **2006**, *124*, 064902.
(30) Pastorino, C.; Kreer, T.; Müller, M.; Binder, K. *Phys. Rev. E* **2007**, *76*, 026706.
(31) Dimitrov, D. I.; Milchev, A.; Binder, K. *J. Chem. Phys.* **2007**, *127*, 084905.
(32) Brinkman, H. C. *Appl. Sci. Res.* **1947**, *A1*, 27.
(33) Succi, S. In *The Lattice Boltzmann Equation for Fluid Dynamics and Beyond*; Oxford University Press: Oxford, U.K., 2001.

stochastic rotational dynamics.[34] Within the small number of investigations that have been carried out with an explicit solvent (see, e.g. refs 23, 25, 28, and 31), systematic studies of the effects neglected in implicit solvent simulations are rare.[25]

In this paper, we study nanotribological aspects of polymer brushes under shear using MD simulations of a classical coarse-grained model. The systems under consideration consist of two opposing polymer brushes under good solvent conditions. We vary the degree of compression, density and length of grafted chains and study static equilibrium properties and Couette flows at various shear rates. The model systems are investigated with and without the presence of explicit solvent molecules. We compare the two cases and draw conclusions about the influence of solvent effects. Using scaling theory, we demonstrate that structural and macroscopic responses of strongly compressed, nonentangled brushes to constant shear motion are characterized by power laws beyond the linear response regime. The numerical results provide reference points for further investigations concerning the response of the here investigated systems to nonstationary shear.

In section II, we present the model and simulation parameters. Section III contains the discussion of our results. First (section IIIA), we analyze the influence of solvent on density profiles, the overlap between the brushes, and the kinetic friction coefficient. We suggest a method to extract a characteristic time scale for a given parameter combination of surface separation, grafting density and chain length (section IIIB) and use the obtained values to perform scaling plots for macroscopic transport properties (section IIIC). In section IV, we present a scaling theory that is capable of explaining our numerical data. Section V shows a comparison to experimental data and other simulations, where solvent effects have been treated differently. We summarize our results in section VI.

II. Model and Parameters

Polymer chains are represented by the Kremer-Grest (KG) model[35], which is a generic coarse-grained model that has been applied in many previous studies.[8,14,15,19,24,26,27,30,29,35−37] In the KG model, monomers interact via the Lennard-Jones (LJ) potential,

$$U_{\mathrm{LJ}}(r_{ij}) = 4\epsilon[(\sigma/r_{ij})^{12} - (\sigma/r_{ij})^{6} - (\sigma/r_{\mathrm{c}})^{12} + (\sigma/r_{\mathrm{c}})^{6}] \qquad (1)$$

where ϵ and σ define the units of energy and length, respectively. r_{ij} denotes the distance between monomer i and j, and r_{c} is the cutoff radius of the potential. We consider a purely repulsive polymer model; i.e., we choose $r_{\mathrm{c}} = 2^{1/6}\sigma$, and shift U_{LJ} to avoid a discontinuous force at the cutoff. The connectivity along the chain backbone is assured via the FENE potential[35]

$$U_{\mathrm{FENE}}(r) = -\frac{1}{2}kr_0^2 \ln[1-(r/r_0)^2] \quad (r < r_0) \qquad (2)$$

where r is the distance between neighboring monomers in a chain, $k = 30\epsilon/\sigma$, and $r_0 = 1.5\sigma$. The equilibrium bond length, $b = 0.97\sigma$, follows from the minimum of $U_{\mathrm{LJ}}(r) + U_{\mathrm{FENE}}(r)$. The KG model prevents bond crossing and yields the characteristic properties of polymer solutions and melts.[35,36]

The polymers are grafted onto a surface with one chain end. The substrates are represented by rigid, face-centered cubic (fcc) crystalline surfaces[38] with area $A = L_xL_y = 42\sigma \times 36.373\sigma = 1527.666\sigma^2$. ($L_x$ and L_y are respectively the extension of the substrate in shear and neutral direction.) We mimic the interaction of monomers and solvent with the wall atoms by eq 1 using the same values for r_{c}, σ, and ϵ as for the monomer−monomer interaction. The only exception concerns the interaction between the grafted end-monomers and the wall atoms, where we increase ϵ by a factor of 100 with respect to the monomer−monomer interaction and make the LJ potential attractive by doubling r_{c}.[39] The wall atoms remain at fixed relative positions and move only with the given shear velocity. Using this approach, we imply chemisorbed polymer chains on a substrate with infinite mass. Periodic boundary conditions are applied parallel to the surfaces.

In many previous simulations,[8,14,15,19,24,26,27,29,30] the solvent was treated implicitly; i.e., the kinetic energy dissipated to the solvent is mimicked by the application of a thermostat. Alternatively, we introduce explicit solvent molecules as LJ dimers, which are connected via eq 2 with the same interaction parameters as for the monomer−monomer interaction. This means that the Flory−Huggins parameter, χ, is zero and hence the excluded volume parameter reads $v \approx a^3(1 - 2\chi) \approx a^3$ (a the effective monomer size). Since v is positive, we have good solvent conditions, independent of the temperature.[40] We use LJ dimers instead of (e.g.) monomers for the solvent in order to hamper packing and to account for rotational and vibrational degrees of freedom. However, our approach does not aim at describing all features of a real solvent but rather attempts to reflect excluded volume and finite inertia effects, as well as the momentum transport of an explicit solvent. A snapshot of a simulated system with explicit solvent at static equilibrium can be seen in Figure 1.

We solve the classical equations of motion via the velocity−Verlet algorithm[41] using a time-step of $\Delta t = 2 \times 10^{-3}\tau_{\mathrm{LJ}}$, where $\tau_{\mathrm{LJ}} = \sigma(m/\epsilon)^{1/2}$ represents the LJ time unit. The particle mass, m, is set to unity for all monomers and solvent particles. We systematically checked that our results remain unchanged when the time-step is reduced to $\Delta t = 5 \times 10^{-4}\tau_{\mathrm{LJ}}$.

Temperature is kept constant at $T = 1.68\epsilon/k_{\mathrm{B}}$ (k_{B} the Boltzmann constant) using a dissipative particle dynamics (DPD) thermostat.[41,44−47] The thermostat adds to the total conservative force on each particle i a dissipative force, $\mathbf{F}_i^{\mathrm{D}}$, and a random force, $\mathbf{F}_i^{\mathrm{R}}$. Both forces are applied in a pairwise form, such that the sum

(34) Malevanets, A.; Kapral, R. *J. Chem. Phys.* **1999**, *110*, 8605. Malevanets, A.; Kapral, R. *J. Chem. Phys.* **2000**, *112*, 7268.
(35) Grest, G. S.; Kremer, K. *Phys. Rev. A* **1986**, *33*, 3628. Kremer, K.; Grest, G. S. *J. Chem. Phys.* **1990**, *92*, 5057.
(36) Kremer, K.; Grest, G. S.; Carmesin, I. *Phys. Rev. Lett.* **1988**, *61*, 566.
(37) Kreer, T.; Metzger, S.; Müller, M.; Binder, K.; Baschnagel, J. *J. Chem. Phys.* **2004**, *120*, 4012.

(38) We take the upper layer of an fcc-crystal, which is equivalent to a two-dimensional hexagonal lattice.
(39) With this method we allow the grafted ends to find their equilibrium positions on the substrate, after their starting positions have been chosen randomly. Sliding of the grafted ends over the substrates is not observed at any of the examined shear rates.
(40) Since the LJ interaction between the monomers is always repulsive, good solvent conditions are guaranteed even under the absence of solvent.
(41) Frenkel, D.; Smit, B. In *Understanding Molecular Simulation*, 2nd edition; Academic Press: San Diego, CA, 2002.
(42) Meyer, H.; Kreer, T.; Cavallo, A.; Wittmer, J. P.; Baschnagel, J. *Eur. Phys. J.—Spec. Top.* **2007**, *141*, 167.
(43) Note that this value of R_{g} corresponds to the extension of a single chain *without* an explicit solvent. With the explicit solvent of our model R_{g} might be different and should depend on the total particle density. From that point of view, the value given for ρ_{g}^* can only be understood as a rough estimate for the critical grafting density.
(44) Hoogerbrugge, P. J.; Koelman, J. M. V. A. *Europhys. Lett.* **1992**, *19*, 155.
(45) Espanol, P. *Phys. Rev. E* **1995**, *52*, 1734.
(46) Espanol, P.; Warren, P. *Europhys. Lett.* **1995**, *30*, 191.
(47) Groot, R. D.; Warren, P. B. *J. Chem. Phys.* **1997**, *107*, 4423.

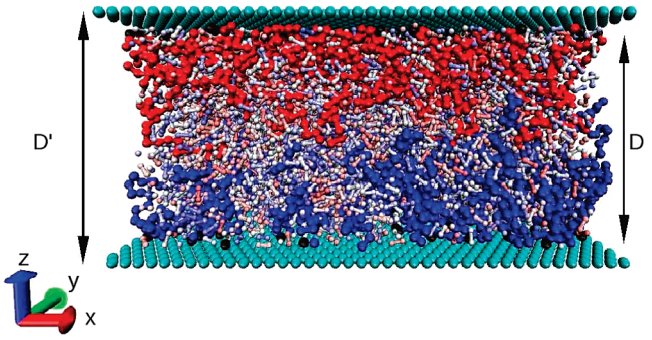

Figure 1. Typical snapshot of two polymer brushes at static equilibrium. The distance between the surfaces (light blue spheres) is $D' \approx 19.7$, corresponding to a distance between grafting planes of $D = 17.5$. Each brush consists of chains with $N = 30$ monomers per chain. The grafting density is approximately twice the critical grafting density, at which the chains overlap. Red and dark blue spheres represent monomers, and white spheres are solvent molecules. Their size has been scaled down for clarity.

of thermostatting forces acting on a particle pair vanishes. With Γ the friction constant, the dissipative force reads

$$\mathbf{F}_i^{\mathrm{D}} = -\Gamma \sum_{j(\neq i)} \omega^{\mathrm{D}}(\mathbf{r}_{ij})(\hat{\mathbf{r}}_{ij} \cdot \mathbf{v}_{ij})\hat{\mathbf{r}}_{ij} \tag{3}$$

where $\hat{\mathbf{r}}_{ij} = (\mathbf{r}_i - \mathbf{r}_j)/r_{ij}$ and $\mathbf{v}_{ij} = \mathbf{v}_i - \mathbf{v}_j$. We choose the commonly employed weight function

$$\omega^{\mathrm{D}}(r_{ij}) = \begin{cases} (1 - r_{ij}/r_{\mathrm{c}})^2 & (r_{ij} < r_{\mathrm{c}}), \\ 0 & (r_{ij} \geq r_{\mathrm{c}}), \end{cases} \tag{4}$$

with the same cutoff range r_{c} as for the LJ interaction. The random force is given by

$$\mathbf{F}_i^{\mathrm{R}} = \lambda \sum_{j(\neq i)} \omega^{\mathrm{R}}(r_{ij})\theta_{ij}\hat{\mathbf{r}}_{ij} \tag{5}$$

where θ_{ij} is a random variable with zero mean, unit variance, and $\theta_{ij} = \theta_{ji}$. $\omega^{\mathrm{R}}(r_{ij})$ denotes the weight function for the random force. Friction and noise strengths, λ, define the temperature via $\lambda^2 = 2k_{\mathrm{B}}T\Gamma$. We choose $\Gamma = 5\tau_{\mathrm{LJ}}^{-1}$ for the friction constant. In ref 28, a larger value ($\Gamma = 12.5\tau_{\mathrm{LJ}}^{-1}$) was chosen. However, we want to avoid overdamping of the dynamics by the thermostat. During the simulation we monitor T and find isothermal conditions for all shear velocities considered here.

The fluctuation−dissipation theorem demands that the weight functions for dissipative and random forces satisfy

$$[\omega^{\mathrm{R}}]^2 = \omega^{\mathrm{D}} \tag{6}$$

The weight function does not necessarily have to be of the specific form of eq 4. Instead one can choose a different function, as long as eq 6 is fulfilled. The strengths and weaknesses of different weight functions have been studied recently for the KG model without explicit solvent[30] and a slightly different model with solvent.[28]

Our simulated chains each consist of $N = 30$ or $N = 60$ monomers. These degrees of polymerization are small enough to avoid entanglements in the bulk.[36] Reference 42 suggests that the entanglement length increases with decreasing thickness of a confined concentrated solution, such that we expect nonentangled chains for all systems under consideration.

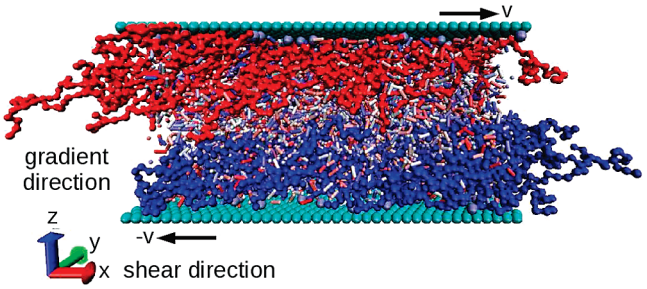

Figure 2. Snapshot of two polymer brushes with the same parameters as in Figure 1, but now at constant relative shear velocity. The shear rate, $\dot{\gamma} \equiv 2v/D$, corresponds to a Weissenberg number of $W \approx 13.5$; i.e., the system is well beyond linear response.

As an additional parameter, we vary the density of grafted chains, ρ_{g}. Our smallest grafting density for $N = 30$ is $\rho_{\mathrm{g}} \approx 1.1\rho_{\mathrm{g}}^*$, where the critical grafting density, $\rho_{\mathrm{g}}^* = 1/\pi R_{\mathrm{g}}^2$, can be extracted from the mean square radius of gyration,

$$R_{\mathrm{g}}^2 \equiv \langle \mathbf{R}_{\mathrm{g}}^2 \rangle \equiv \frac{1}{N} \left\langle \sum_i (\mathbf{r}_i - \mathbf{r}_{\mathrm{cm}})^2 \right\rangle \tag{7}$$

of isolated chains in solution.[43] Here, $\mathbf{r}_{\mathrm{cm}}$ denotes the chain's center-of-mass position vector and the average is taken over all simulated chains. With $\rho_g \approx \rho_g^*$, we consider a system just at the mushroom-to-brush crossover. We systematically increase ρ_{g} to a maximum value of $\rho_g \approx 4.4\rho_g^*$, where we expect semidilute polymer brushes.[37] For $N = 60$ we consider two grafting densities, which correspond to $\rho_g \approx 1.1\rho_g^*(N = 30)$ and $\rho_g \approx 2.2\rho_g^*(N = 30)$, respectively.[48]

Shear is performed at fixed distances between the surfaces, D'. In the following, we characterize the compression of the bilayer by the (mean) distance between the grafting planes, $D = D' - 2r_{\mathrm{c}} = D' - 2 \times 2^{1/6}\sigma$. With $D = 12\sigma$, $D = 14.75\sigma$, and $D = 17.5\sigma$, we consider three different degrees of compression. Depending on N and ρ_{g}, this corresponds to compressions between $2h/D \approx 2$ and $2h/D \approx 6.5$ relative to the height h of a single, uncompressed brush without explicit solvent.[37] Upon varying the parameter D', we adjust the number of solvent dimers such that the overall particle number density remains at a constant value of $\rho = 0.9$.

III. Results and Discussion

In this section, we present data for two compressed, opposing polymer brushes under lateral steady-state motion of the adsorbing substrates. We consider stationary Couette flows, which are applied by shearing the substrates with a constant relative velocity of $2v$ at fixed distance D. The corresponding shear rate is defined as $\dot{\gamma} \equiv 2v/D$. All quantities are presented in LJ units.

A. The Influence of Solvent. A snapshot of a typical configuration at constant shear velocity is depicted in Figure 2. We observe that the brushes overlap and the solvent concentration is high between the two brushes and, perhaps less clearly, also at the surfaces. The majority of chains seems to incline along the shear direction, although some chains tilt in the opposite direction due to fluctuations. An analysis of monomer and solvent density profiles (Figure 3) reveals that solvent molecules accumulate at the substrates (seen also in a related model[31]) and in the interface of the two brushes, even in static equilibrium. Under shear the

(48) For convenience, we express the grafting density for $N = 60$ in terms of ρ_{g}^* for $N = 30$. Since $\rho_{\mathrm{g}} \approx 1.1\rho_{\mathrm{g}}^*(N = 30)$ is much larger than the critical grafting density for $N = 60$, we have semidilute polymer brushes at both grafting densities of $N = 60$.

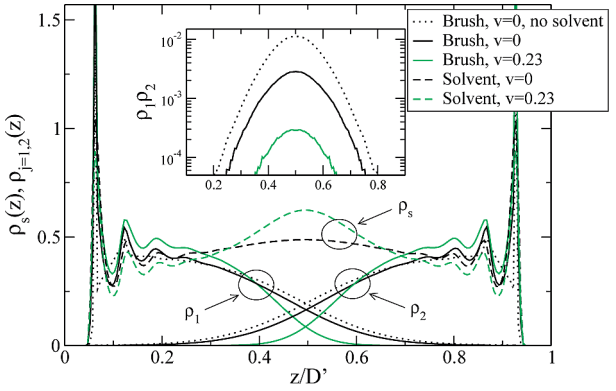

Figure 3. Monomer and solvent density profiles at distance $D = 12$ between grafting planes for chains of length $N = 30$. The grafting density is $\rho_g \approx 2.2\rho_g^*$ for all systems. We show data for a solvent-free case (dotted lines) and the corresponding system with explicit solvent molecules. Static equilibrium (black lines) is compared to steady state motion at our largest shear velocity, $v = 0.23$ (green lines). The inset shows a semilogarithmic plot of the overlap between the brushes, which can be quantified by the area under $\rho_1(z)\rho_2(z)$ (see text).

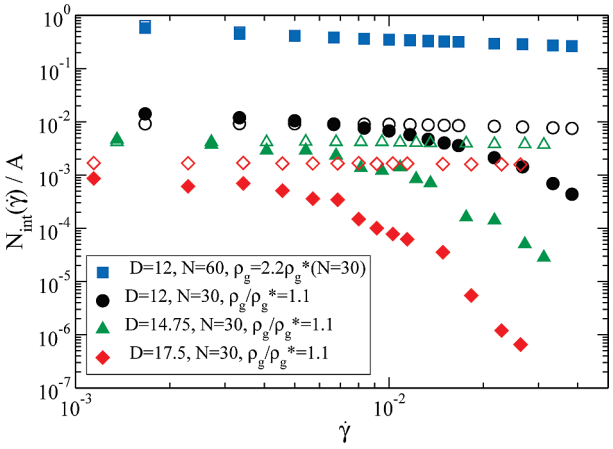

Figure 4. Number of binary interactions between brushes as a function of shear rate on a double−logarithmic scale. For the different systems under consideration, N_{int} varies over almost 3 orders of magnitude in static equilibrium (not shown). Responses to shear reach from almost constant N_{int} to strongly decreasing overlap. Solvent (filled symbols) and solvent-free cases (open symbols) behave very differently at small grafting density and larger distances. For our largest compression [$D = 12$, $N = 60$, $\rho_g = 2.2\rho_g$ ($N = 30$)], no differences between the two cases are observed.

brushes become more dense and squeeze solvent molecules into the interfacial region between the brushes. The total density (not shown) of the confined liquid, however, remains constant. This implies that shear does not induce density fluctuations; the system keeps its low compressibility. When solvent molecules are explicitly considered, the overall density and hence the pressure normal to the substrates (z-direction) is larger compared to the solvent-free case of our model. The corresponding solvent-free systems therefore exhibit a larger brush thickness, both in static equilibrium and under shear, as already observed in ref 25.

The inset of Figure 3 demonstrates that the overlap between brushes with explicit solvent is reduced compared to solvent-free cases. Furthermore, we observe that, under sufficiently strong shear, the layer thickness decreases and this leads to a reduced interpenetration between the brushes. The latter can be quantified by an overlap integral[24,30]

$$I_{ov}(\dot{\gamma}) \sim \int \mathrm{d}z\, \rho_1(z)\rho_2(z) \tag{8}$$

where $\rho_j(z)$ represents the density profile of brush j (= 1,2). Note that $I_{ov}(\dot{\gamma})$ is proportional to the number of binary interactions between monomers of different brushes, N_{int}, as has been demonstrated in a previous study.[24] Various numerical investigations[24−27,29,30] have shown that shear thinning coincides with a reduced overlap between the grafted layers and indicated that macroscopic transport properties, e.g., the shear viscosity, are correlated to $I_{ov}(\dot{\gamma})$.

While the overlap integral, in principle, may be measurable experimentally, we can straightforwardly count the number of binary interbrush interactions in our simulation, which is much easier than the integration of the density profiles. Figure 4 shows N_{int} as a function of shear rate for different parameter combinations (ρ_g, D, N).[49] Not only the equilibrium values (not shown) but also the responses of N_{int} to shear are very different for the various systems under consideration. Systems with explicit solvent and their solvent-free counterparts reveal distinct differences in their responses, in particular at small grafting densities and larger surface separations, where solvent effects are important. When dragged through an explicit solvent, the chains feel stronger forces than for the solvent-free case. The overlap therefore reduces at smaller shear rates.

A qualitatively different behavior of solvent and solvent-free systems can be observed for the kinetic friction coefficient, μ. We define μ as the ratio between shear and normal forces

$$\mu(\dot{\gamma}) = \frac{f_x(\dot{\gamma})}{f_z(\dot{\gamma})} \tag{9}$$

which we apply to the center-of-mass of the confining substrates to maintain constant v and D. We verified that our results are independent of whether we characterize the macroscopic response by measuring forces at the substrate or by calculating elements of the stress tensor, using the Irving−Kirkwood method.[50]

All systems keep their low compressibility even under strong shear. Therefore, f_z remains almost independent of $\dot{\gamma}$, and only at our largest velocities we find (for some cases) a small increase of f_z by approximately 4%.

The kinetic friction coefficient is shown in Figure 5 for $D = 12$ and $N = 30$. We observe an increase of μ with shear rate that is particularly strong for solvent-free systems, which exhibit larger friction coefficients at all investigated grafting densities. This observation, which is in agreement with the conclusions drawn in ref 25, highlights the importance of solvent effects in polymer-brush lubrication.

The presence of explicit solvent does not only lead to smaller values of μ. For solvent-free systems, μ decreases for larger grafting densities due to larger normal forces. Since solvent and solvent-free cases merge at large values of ρ_g, the kinetic friction coefficient has to increase with grafting density for systems with solvent. The arrows in Figure 5 indicate the behavior for both cases.

However, in the following we will demonstrate that it is possible to describe both cases on the basis of the same analytical concept. To this purpose we extract a characteristic time scale and the related length scale, which determine the response of a given system to shear. We suggest a method to obtain the time scale,

(49) N_{int} has to be understood as the number of binary LJ interactions at a given time step. We obtain a continuous value for N_{int} after averaging.

(50) Irving, J. H.; Kirkwood, J. G. *J. Chem. Phys.* **1950**, *18*, 817.

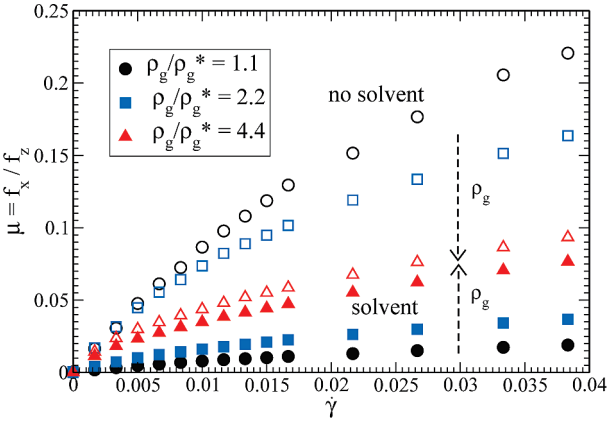

Figure 5. Kinetic friction coefficient, defined as the ratio between shear and normal forces measured at the substrates, as a function of shear rate ($D = 12$, $N = 30$). Note that systems without an explicit solvent (open symbols) reveal a significantly larger friction coefficient than systems with solvent particles (filled symbols). For large grafting densities, ρ_g, the two cases have to merge, which means that μ decreases with ρ_g for solvent-free systems, while it increases for systems with solvent.

where we assume that the mean extension of a grafted chain in shear direction represents a relevant length scale.

B. Determination of the Weissenberg Number Using Shear-Induced Chain Deformation. The chain extension may be characterized by the radius of gyration [eq 7] for different shear rates $\dot{\gamma}$. Figure 6 shows the ratio

$$q_\alpha \equiv \frac{R_{g,\alpha}^2(\dot{\gamma})}{R_{g,\alpha}^2(0)} \tag{10}$$

in shear ($\alpha = x$) and gradient ($\alpha = z$) directions for various degrees of compression, grafting densities, and two different chain lengths as a function of the Weissenberg number, $W \equiv \dot{\gamma}/\dot{\gamma}^*$. Here, $\dot{\gamma}^*$ denotes the critical shear rate, which can be regarded as an inverse relaxation time of the bilayer.

The determination of W, i.e., of $\dot{\gamma}^*$, is crucial for the discussion of our results. Linear response should apply for small values of W, while nonlinear effects are important for large values. However, the precise scale for W is somewhat arbitrary, because the bilayer has a broad spectrum of relaxation times, and it is not clear which of them is best suited. Therefore, it is convenient to use an operational definition that sets the scale for W. Here, we determine $\dot{\gamma}^*$ operationally by plotting the raw data for q_x against $\dot{\gamma}$ and shifting the data such that a master curve results. The fact that this procedure yields an (almost) perfect data collapse (Figure 6) is a nontrivial result because the raw data strongly differ from each other. The values for $\dot{\gamma}^*$ and $R_{g,\alpha}^2(0)$ are compiled in Table 1 for all considered parameter combinations.

Figure 6 shows that q_z decreases only weakly for $W > 1$. The chain extension in the gradient direction saturates at different values of W, depending on the chosen parameters (ρ_g, D, N), due to the finite compressibility of the grafted layers.

In agreement with early studies of Murat and Grest,[14] we find a pronounced stretching of the chains along the shear direction beyond the linear response regime. The data do not reach the limit of fully extended chains, where q_x should become constant. Instead, we obtain a universal power law

$$q_x \sim W^\phi \tag{11}$$

for Weissenberg numbers $W > 1$. The exponent $\phi \approx 0.5$ (indicated by straight lines) is derived analytically in section IV.

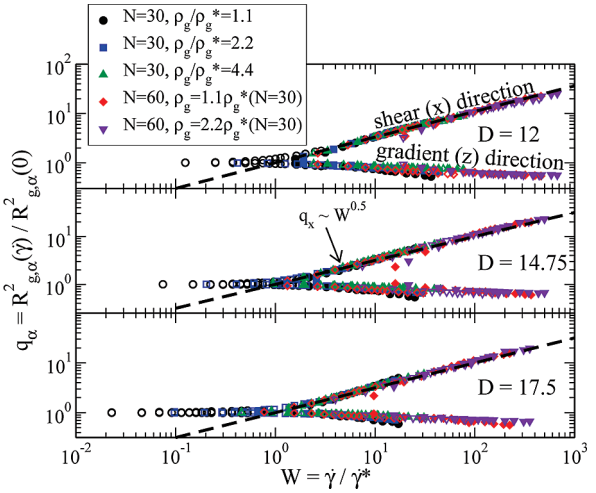

Figure 6. Double−logarithmic scaling plot for the chain extension in shear (x) and gradient (z) directions as a function of the Weissenberg number for $D = 12$, $D = 14.75$, and $D = 17.5$ (from above). Data is shown for $N = 30$ at three grafting densities and for $N = 60$ at two similar values of ρ_g. We obtain no chain deformation for $W \leq 1$. Upon increasing W, the grafted layers shrink slightly and remain at constant height for larger shear rates. The chains stretch in shear direction, following a universal power-law (indicated by straight lines). Solvent (filled symbols) and solvent-free cases (open symbols) can be brought onto the same master curve, as data for different values of D (not shown).

Table 1. Mean Square Radius of Gyration, $R_{g,\alpha}^2(0)$, in Shear ($\alpha = x$) and Gradient ($\alpha = z$) Directions, Critical Shear Rate, $\dot{\gamma}^*$, and Critical Force, $f_x(\dot{\gamma}^*)$[a]

D	N	$\rho_g/\rho_g^*(N = 30)$	solvent	$R_{g,x}^2$	$R_{g,z}^2$	$\dot{\gamma}^* \times 10^4$	$f_x(\dot{\gamma}^*)$
12	30	1.1	+	2.78	3.17	10.5	25.5
	30	2.2	+	2.58	3.28	8.70	40.2
	30	4.4	+	2.37	3.42	5.00	69.4
	60	1.1	+	5.41	4.88	0.83	11.8
	60	2.2	+	4.26	4.69	0.57	15.3
	30	1.1	−	3.42	3.80	133	18.6
	30	2.2	−	2.98	3.68	40.0	37.3
	30	4.4	−	2.44	3.48	6.90	72.7
	60	1.1	−	6.58	5.19	6.25	12.7
	60	2.2	−	4.92	4.77	0.87	21.8
14.75	30	1.1	+	2.71	3.56	12.5	24.2
	30	2.2	+	2.51	3.96	10.5	39.2
	30	4.4	+	2.26	4.50	6.90	66.4
	60	1.1	+	5.11	5.59	0.85	10.5
	60	2.2	+	4.22	5.43	0.63	18.0
	30	1.1	−	3.37	4.59	182	13.9
	30	2.2	−	2.97	4.67	66.7	31.2
	30	4.4	−	2.49	4.66	14.3	72.8
	60	1.1	−	7.16	6.49	10.3	12.7
	60	2.2	−	5.17	5.83	1.82	21.8
17.5	30	1.1	+	2.56	3.61	15.4	24.6
	30	2.2	+	2.48	4.44	16.7	41.3
	30	4.4	+	2.12	5.57	8.51	66.4
	60	1.1	+	5.40	6.69	1.18	21.8
	60	2.2	+	4.44	6.55	0.74	15.6
	30	1.1	−	3.21	5.44	500	9.6
	30	2.2	−	2.85	5.94	118	27.8
	30	4.4	−	2.49	6.13	25.0	69.4
	60	1.1	−	7.16	7.53	14.8	12.7
	60	2.2	−	5.50	7.02	2.86	21.8

[a] See Figure 9 for the different parameter combinations under consideration: distance D between grafting planes, chain length N, and ratio between grafting density and (approximate) critical grafting density for chains of length $N = 30$ (+ and − respectively denote systems with and without explicit solvent).

Inspection of Table 1 shows that the lateral chain extension at equilibrium decreases upon increasing grafting density. The opposite behavior is observed for the direction perpendicular to the surfaces. As expected, the brush thickness decreases under compression.

Larger values of $\dot{\gamma}^*$ are obtained for solvent-free systems compared to systems with explicit solvent, which indicates that the latter leave linear response earlier due to the additional monomer−solvent friction.

A similar observation can be made for the surface separation. With decreasing compression, i.e., larger values of D, we systematically find larger critical shear rates. The force that drives the system out of the linear-response regime increases with compression. This observation agrees with previous simulations[23] and experiments.[13]

Increasing the chain length at fixed D and grafting density leads to a larger frictional force per chain. Moreover, larger chains need more time to relax. Systems with $N = 60$ thus leave the regime of linear response earlier than those with $N = 30$.

Interestingly, the structural response in shear direction is universal, independent of whether the solvent is explicitly included or not. We attribute this finding to the fact that the DPD thermostat fulfills Newton's third law and thus accounts for hydrodynamic correlations, at least at large polymer concentrations. For semidilute polymer solutions, Zimm dynamics has been observed on small time scales.[51]

Finally, we point out that the same results are obtained when we define q_α via the mean square end-to-end distance instead of using $R_{g,\alpha}^2$.

C. Viscosity and Shear Force. To perform scaling plots for the transport properties, it is not sufficient to know the critical shear rate. For instance, to plot the ratio

$$s \equiv \frac{\eta_{xz}(\dot{\gamma})}{\eta_{xz}(0)} \tag{12}$$

where $\eta_{xz}(\dot{\gamma})$ represents the shear viscosity, we need $\eta_{xz}(0)$ for each examined system. The (collective) zero-shear viscosity is difficult to compute numerically. The measurements have to be performed at small shear rates and this is related to a bad signal-to-noise ratio.

However, in principle we can calculate $\eta_{xz}(0)$ from the data presented in Table 1: In the linear response regime, the Weissenberg number may be expressed via the acquired energy per chain,

$$W \approx \frac{f_x(\dot{\gamma}) R_{g,x}(0)}{N_g k_B T} \tag{13}$$

where $f_x(\dot{\gamma})$ denotes the shear force acting on the substrate, N_g is the number of grafted chains and $R_{g,x}(0) \equiv R_{g,x}^2(0)^{1/2}$. The critical shear rate can be found from the requirement that the acquired energy is comparable to $k_B T$, i.e. when W is of order unity. The shear force is proportional to $\dot{\gamma}$ in linear response. With the zero-shear viscosity

$$\eta_{xz}(0) = \frac{f_x(\dot{\gamma})}{A\dot{\gamma}} \quad (W \leq 1) \tag{14}$$

one thus may write

$$\dot{\gamma}^* \approx \frac{\rho_g k_B T}{\eta_{xz}(0) R_{g,x}(0)} \tag{15}$$

where we have used $\rho_g = N_g/A$.

(51) Ahlrichs, P.; Everaers, R.; Duenweg, B. *Phys. Rev. E* **2001**, *64*, 040501.

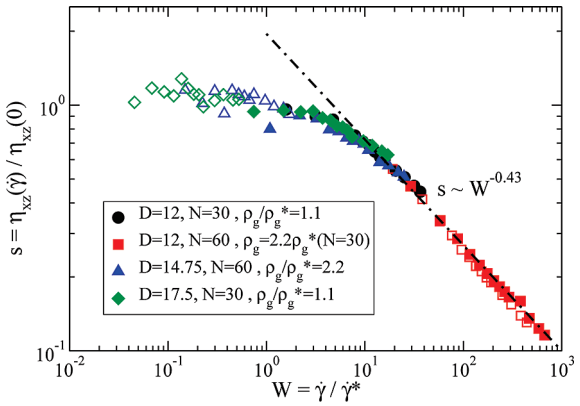

Figure 7. Double−logarithmic scaling plot for the shear viscosity as a function of the Weissenberg number. We show examples for systems with explicit solvent (filled symbols) and their solvent-free counterparts (open symbols). The normalization constant, $\eta_{xz}(0)$, follows from shifting the data along the ordinate, such that $s \to 1$ for $W \ll 1$.

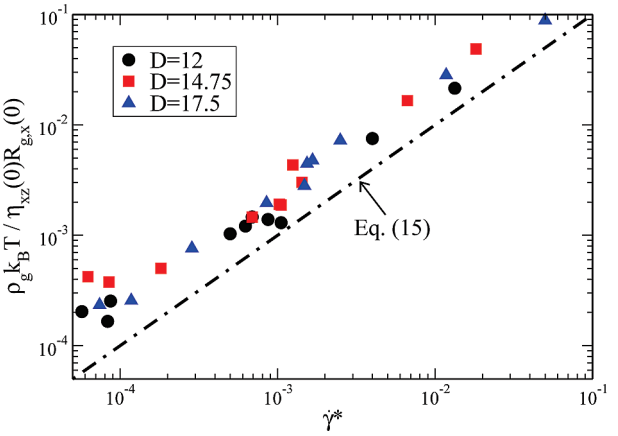

Figure 8. Numerical test of eq 15. The chain extension in static equilibrium, $R_{g,x}(0)$, has directly been measured in the simulation and the zero-shear viscosity is identified as the plateau value of $\eta_{xz}(\dot{\gamma})$ at small shear rates (or by extrapolation of the data, where a plateau was not clearly visible). The critical shear rate, $\dot{\gamma}^*$, is taken from Table 1.

Equation 15 provides the possibility to compute $\eta_{xz}(0)$ for a given critical shear rate up to a (constant) numerical factor. Unfortunately, when plotting the ratio s, we find strong statistical fluctuations. Therefore, we use a different way of presentation by shifting the data along the ordinate to obtain an estimate for the zero-shear viscosity. Figure 7 shows an example for some cases.[52]

Using the values we obtained for $\dot{\gamma}^*$ in the previous paragraph, it is possible to achieve a reasonable data collapse. This again is a nontrivial result, which indicates a strong correlation between the deformation of chains and the macroscopic response. Beyond linear response the data follow a power-law,

$$s \sim W^\zeta \quad (W > 1) \tag{16}$$

The exponent $\zeta = -0.43$ (indicated by a straight line) can be derived analytically, as we will demonstrate in section IV.

The values for $\eta_{xz}(0)$ used in Figure 7 can be cross-checked with eq 15. Taking $\dot{\gamma}^*$ and $R_{g,x}(0)$ from Table 1, we find a reasonable

(52) $\eta_{xz}(\dot{\gamma})$ is determined from $\eta_{xz}(\dot{\gamma}) = \sigma_{xz}(\dot{\gamma})/(\dot{\gamma})$, where the shear stress, $\sigma_{xz}(\dot{\gamma})$, is calculated from the Irving−Kirkwood formula.[50]

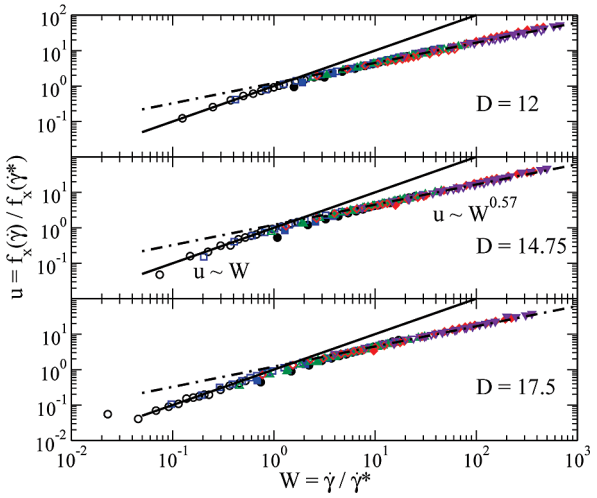

Figure 9. Double−logarithmic scaling plot for the shear force as a function of the Weissenberg number (same legend as in Figure 6). Data is shown for two chain lengths and different surface coverage at distances $D = 12$, $D = 14.75$, and $D = 17.5$ between grafting planes. Filled symbols represent systems with explicit solvent, open symbols are solvent-free systems. The normalization constant, $f_x(\dot{\gamma}^*)$, is obtained by shifting the data along the ordinate such that $u = 1$ for $W = 1$. The values are compiled in Table 1.

agreement with eq 15 up to a numerical factor of about 2, as can be seen from Figure 8. However, the data reveal strong fluctuations, which explains why it is almost impossible to produce a successful scaling plot for s from the direct calculation of $\eta_{xz}(0)$.

Plotting the shear viscosity always reveals strong fluctuations at small shear rates. A somewhat clearer picture is obtained from the analysis of the shear force. Here, we measure $f_x(\dot{\gamma})$ at the substrates. Figure 9 shows the ratio

$$u \equiv \frac{f_x(\dot{\gamma})}{f_x(\dot{\gamma}^*)} \tag{17}$$

as a function of W for all considered parameter combinations. The data collapse is even better than for the viscosity. As expected, u scales linearly with W for $W \leq 1$. Beyond linear response we obtain a power-law,

$$u \sim W^{\kappa} (W > 1) \tag{18}$$

The dashed-dotted lines represent an exponent of $\kappa = 1 + \zeta = 0.57$, which follows from

$$s \sim \frac{f_x(\dot{\gamma})}{f_x(\dot{\gamma}^*)} W^{-1} \Rightarrow u \sim sW \tag{19}$$

The values for $f_x(\dot{\gamma}^*)$ are obtained by shifting the data along the ordinate, such that $u(W = 1) = 1$. For the same reason as before, we do not get a satisfying scaling plot when using the relation

$$f_x(\dot{\gamma}^*) \approx \frac{N_g k_B T}{R_{g,x}(0)} \tag{20}$$

which follows from eq 13 for $W = 1$.

So far we have shown that the lateral extension of the grafted chains (q_x) and the macroscopic response (viscosity s and shear force u) are characterized by the same time scale, $1/\dot{\gamma}^*$. Beyond linear response we find that q_x, s, and u are power-laws of the Weissenberg number. In the following, we present a theoretical approach to determine the critical shear rate as a function of N, ρ_g, and D, which allows us to calculate the exponents ϕ and κ.

IV. Scaling Theory

The data previously presented in this paper correspond to brushes with compressions $2h/D \geq 2$ (see section II). We verified furthermore, from equivalent plots as shown in Figure 3, that the sum of the monomer density profiles, $\rho_1(z) + \rho_2(z)$, is constant in the center between the substrates for (almost) all considered shear rates. Therefore, in the following, we assume strongly compressed brushes ($2h/D \geq 2$) with a uniform monomer concentration, $c \sim N\rho_g/D$, in the overlap region. We will use this feature below for the linear response regime.

The starting point of our scaling approach is the interpenetration depth, δ, i.e. the overlap thickness of the bilayer. We first consider molten brushes. The overlap thickness can be derived from the change in free energy, ΔF, when a chain segment of length δ is pushed into the opposing layer. Witten et al.[53] demonstrated that ΔF can be written as

$$\Delta F \sim \left(-\frac{\delta^3 \partial \Phi(z)}{a^2 \quad \partial z} \right)^{1/2} \tag{21}$$

where the molecular field, $\Phi(z)$, may be of the classical parabolic form[54]

$$\Phi(z) = \Phi_0 - \frac{1}{2}\left(\frac{\pi z}{2Na}\right)^2 \tag{22}$$

with Φ_0 constant. In equilibrium, ΔF is of the order $k_B T$. We take the derivative of $\Phi(z)$ at the middle of the bilayer, $z = D/2$, and obtain from eq 21

$$\delta \sim \left(\frac{N^2 a^4}{D}\right)^{1/3} \tag{23}$$

for the interpenetration depth of strongly compressed, molten bilayers.[55]

A. Semidilute Brushes with Zimm Dynamics. Let us now consider semidilute brushes. In this case, a brush may be considered as a dense melt of concentration blobs.[56] Therefore, eq 23 still holds with the replacements

$$N \rightarrow N/g_c, \quad a \rightarrow \xi_c \tag{24}$$

where

$$\xi_c \sim a(ca^3)^{\nu/(1-3\nu)} \tag{25}$$

(53) Witten, T. A.; Leibler, L.; Pincus, P. A. *Macromolecules* **1990**, *23*, 824.
(54) Milner, S. T.; Witten, T. A.; Cates, M. E. *Macromolecules* **1988**, *21*, 2610. *Europhys. Lett.* **1988**, *5*, 413.
(55) Equation (23) is similar to the expression found by Witten et al.[53]

$$\delta \sim \left(\frac{N^2 a^4}{h}\right)^{1/3}$$

where D is replaced by the unperturbed brush height. The difference occurs because in ref 53 the derivative of $\Phi(z)$ is taken at $z = h$, which hence characterizes the behavior of two brushes just coming into contact.
(56) De Gennes, P. G. *Scaling Concepts in Polymer Physics*; Cornell University Press: New York, 1979.

represents the size of the concentration blob consisting of $g_c \sim (\xi_c/a)^{1/\nu}$ monomers and $\nu \approx 0.588$ is the Flory-exponent. With the uniform concentration $c \sim N\rho_g/D$, eq 23 yields

$$\delta \sim a\left[N^{2\nu}(\rho_g a^2)^{2(1-2\nu)}\left(\frac{a}{D}\right)^{1-\nu}\right]^{1/(3\nu-1)} \quad (26)$$

for the interpenetration depth of strongly compressed, semidilute brushes. Under melt conditions, the lateral extension of a chain is given by $R_{g,x}(0) \sim N^{1/2}a$. With eq 24 we get

$$R_{g,x}(0) \sim \left(\frac{N}{g_c}\right)^{1/2}\xi_c \sim a\left[N^{\nu}\left(\frac{D}{\rho_g a^3}\right)^{2\nu-1}\right]^{1/2(3\nu-1)} \quad (27)$$

for semidilute brushes.

In the next step, we estimate the friction force per unit area (f_x/A) in the linear response regime by assuming Zimm dynamics in the blob.[56] Since there are $c\delta/g_c$ blobs (per unit area) in the overlap region, each having a friction coefficient $\eta_s\xi_c$ (η_s the solvent viscosity), and a typical velocity is $\dot\gamma D$, we may write

$$\frac{f_x(\dot\gamma)}{A} \sim \frac{c\delta}{g_c}\eta_s\xi_c\dot\gamma D \quad (W \le 1) \quad (28)$$

With eqs 25 and 26 this leads to[57]

$$f_x(\dot\gamma) \sim \left[N^{8\nu}(\rho_g a^2)^{2(1+\nu)}\left(\frac{a}{D}\right)^{4(\nu-1)}\right]^{1/(3\nu-1)}\eta_s\dot\gamma A \quad (29)$$

in the linear response regime.

We anticipate that thermal fluctuations allow the chains of a brush to exchange between the overlap region and deeper layers.[58] Hence, the shear stress should be sustained by more chains than only those that are in the overlap region at a given time. For the sake of simplicity we do not discuss the structure of the sheared layer in details here. We rather characterize the lateral chain extension averaged over the whole layer. This is formally equivalent to the assumption that all chains sustain the stress equally. We will come back to this point later.

In the following, we determine the critical shear rate by requiring $W = 1$. Let us recall that in the linear regime the transverse free end fluctuations are equilibrium fluctuations. For increasing shear force there is a spontaneous symmetry breaking when the work of the shear force over the typical fluctuations exceeds the thermal energy. At higher shear rates the chains are deflected in the shear direction (only). Our definition of W follows from this criterion.

The critical shear rate follows from eq 13 with $W = 1$. Using $\rho_g = N_g/A$ with eqs 27 and 29, we find

$$\dot\gamma^* \sim \frac{k_B T}{\eta_s a^3}\left[N^{-19\nu}(\rho_g a^2)^{20\nu-13}\left(\frac{a}{D}\right)^{14\nu-11}\right]^{1/6(3\nu-1)} \quad (30)$$

or, with $\nu \approx 0.588$, $\dot\gamma^* \sim N^{-2.44}\rho_g{}^{-0.27}D^{0.6}$. For the shear force at $W = 1$, eqs 20 and 27 yield

$$f_x(\dot\gamma^*) \sim \frac{N_g k_B T}{a}\left[N^{-\nu}\left(\frac{\rho_g a^3}{D}\right)^{2\nu-1}\right]^{1/2(3\nu-1)} \quad (31)$$

Note that care has to be taken if one wishes to compare eqs 30 and 31 to the data presented in Table 1. We expect deviations that stem from a dependence of the effective solvent viscosity and monomer size upon a variation of compression and molecular parameters, because η_s and a depend on solvent and monomer density, hence implicitly on N, ρ_g, and D.

We now address the regime beyond linear response. At large shear rates, the chains stretch in the shear direction, such that $R_{g,x}(\dot\gamma) \sim N$. With eq 27 we obtain [see eq 10]

$$q_x \sim N^{(2-5\nu)/(1-3\nu)} \quad (W > 1) \quad (32)$$

On the other hand, eq 30 yields

$$W \sim \dot\gamma^{*-1} \sim N^{19\nu/6(3\nu-1)} \quad (33)$$

such that

$$q_x \sim W^{6(5\nu-2)/19\nu} \quad (W > 1) \quad (34)$$

With $\nu \approx 0.588$ we obtain $\phi \approx 0.5$ [see eq 11], which is in very good agreement with our numerical data in Figure 6.

For strongly stretched chains, we expect the shear force to be proportional to the total number of monomers ($\sim N_g N$) and the typical velocity, i.e.

$$f_x(\dot\gamma) \sim N_g N\dot\gamma D \sim N \quad (W > 1) \quad (35)$$

Hence, upon inserting eqs 31 and 35 into eq 17, one finds

$$u \sim N^{(2-7\nu)/2(1-3\nu)} \quad (36)$$

for the regime beyond linear response. In combination with eq 33, this yields

$$u \sim W^{3(7\nu-2)/19\nu} \quad (W > 1) \quad (37)$$

and with eq 19

$$s \sim W^{-2(3-\nu)/19\nu} \quad (38)$$

Using $\nu \approx 0.588$ we obtain $\kappa \approx 0.57$ [eq 18] and $\zeta \approx -0.43$ [eq 16], which agrees well with the data in Figures 7 and 9.

B. Dry Brushes. So far we have demonstrated that our data can be described by scaling theory, where we assumed strongly

(57) This result is different from the original calculation by Klein,[11] who obtains

$$f_x(\dot\gamma) \sim h\rho_g^{1/2}\left(\frac{h}{D}\right)^{2/3(3\nu-1)}\eta_s\dot\gamma A \quad (W \le 1)$$

Note that this expression can be transformed into

$$f_x(\dot\gamma) \sim \left[N^{9\nu-1}(\rho_g a^2)^{(7\nu-1)/2\nu}\left(\frac{a}{D}\right)^2\right]^{1/3(3\nu-1)}\eta_s\dot\gamma A$$

when the relation $h \sim aN(\rho_g a^2)^{(1-\nu)/2\nu}$ [37] is used. A comparison with eq 29 reveals an almost identical exponent for N, but different scaling-laws for ρ_g and D. We attribute these deviations to the fact that Klein starts out from

$$\delta \sim \rho_g{}^{-1/2}\left(\frac{h}{D}\right)^{1/3}$$

which rather describes the interpenetration for weakly compressed, molten brushes, and to a different estimate of the number of blobs in the interpenetration zone. However, since we base the following scaling argument on the N-dependence of the shear force, Klein's approach would lead to minor differences.

(58) Clement, F.; Charitat, T.; Johner, A.; Joanny, J.-F. *Europhys. Lett.* **2001**, *54*, 65.

compressed, semidilute brushes and included hydrodynamic interactions. Since the simulated systems are fairly dense, another plausible model assumption could have been that hydrodynamic interactions are fully screened and that the monomers obey Rouse dynamics instead of Zimm dynamics. It is therefore important to verify that this assumption of "dry" brushes yields values for the exponents ϕ, κ, and ζ which are in worse agreement with the simulation data in order to lend further credence to the analysis of section IVA. This is what we want to show here.

In the following, we distinguish two cases, a molten brush, where in addition to hydrodynamic interactions also the excluded volume interactions are screened ($\nu = 1/2$), and a semidilute brush consisting of excluded volume blobs as in Sec. IV A.

For brushes without hydrodynamic interactions, the friction force reads [instead of eq 28]

$$f_x(\dot{\gamma}) \sim c\delta\psi\dot{\gamma}DA \quad (W \leq 1) \tag{39}$$

where ψ is a friction coefficient.

We first consider molten brushes. In this regime, eqs 23 and 39 yield

$$f_x(\dot{\gamma}) \sim N^{5/3} \quad (W \leq 1) \tag{40}$$

Since $R_{g,x}(0) \sim N^{1/2}$ under melt conditions, we find with $R_{g,x}(\dot{\gamma}) \sim N$ and eq 13

$$\dot{\gamma}^* \sim \frac{k_B T}{\psi a^2} N^{-13/6} \left(\frac{D}{a}\right)^{1/3} \tag{41}$$

In the nonlinear regime, this yields

$$q_x \sim N \sim W^{6/13} \quad (W > 1) \tag{42}$$

for the chain extension, i.e. $\phi \approx 0.46$. With $f_x^{\mathrm{melt}}(\dot{\gamma}) \sim N$ at large shear rates and $f_x(\dot{\gamma}^*) \sim 1/R_{g,x}(0)$ [eq 13], we find

$$u \sim N^{3/2} \sim W^{9/13} \quad (W > 1) \tag{43}$$

for the shear force, i.e. $\kappa \approx 0.69$. Both predictions for ϕ and κ are not well compatible with our simulation data (Figures 7 and 9), as anticipated above.

Finally, we consider semidilute brushes without hydrodynamic interactions. Although this case appears awkward from an experimental point of view, it can be compared to numerical approaches where hydrodynamic interactions are not taken into account, e.g., due to specific thermostat implementations. We will address one example in the next section.

When the chains are swollen, the interpenetration length is given by eq 26. With eq 39, the shear force for dry, semidilute brushes in linear response scales as

$$f_x(\dot{\gamma}) \sim N^{(11\nu-3)/3(3\nu-1)} \quad (W \leq 1) \tag{44}$$

The critical shear rate follows from eqs 13 and 27, such that

$$\dot{\gamma}^* \sim \frac{k_B T}{\psi a^2} \left[N^{6-25\nu} (\rho_g a^2)^{7(2\nu-1)} \left(\frac{a}{D}\right)^{8\nu-5} \right]^{1/6(3\nu-1)} \tag{45}$$

Beyond linear response this yields, together with eq 32

$$q_x \sim W^{6(5\nu-2)/(25\nu-6)} \quad (W > 1) \tag{46}$$

for the lateral chain extension, i.e., $\phi \approx 0.65$. The scaling of u with W follows from eqs 36 and 45, such that

$$u \sim W^{3(7\nu-2)/(25\nu-6)} \quad (W > 1) \tag{47}$$

i.e., $\kappa \approx 0.73$.

We expect deviations from our approach for weaker compression, when the distance between the grafting planes exceeds h, such that the assumption of a uniform concentration is no longer valid. This regime was considered in ref 59 for molten brushes, where a disentanglement instability is predicted for a critical shear rate. This points in the same direction as the shear thinning we observe. It is to be noted that extrapolating from the strong to the weak overlap regime reveals a minimum in the interpenetration depth.

The above results are built on the chain deformation averaged over the entire layer. The critical shear rate we obtained does not correspond to any simple characteristic frequency. As a matter of fact, the structure of the sheared layer is more complex than reflected by averaged deformations. Chain deformation takes place in the interface and is subsequently transported deeper into the layer by longitudinal chain-end diffusion, which leads to chain-end exchange between the interface and the bulk of the layers. Because the lateral deformation relaxes in the same time, deformed chains are hardly found far away from the interface. Though chains that reside temporarily rather than permanently in the interface are less deformed and chains outside the interface are deformed to some extent as well, chain-end exchange does not distribute the chain deformation evenly across the layer. It seems more natural to base our argument to determine the critical shear rate on the more deformed chains located in (and close to) the interface at a given time. In the compressed brush, chain ends are only weakly localized in the interface, in contrast to an Alexander brush. This is discussed in detail in the appendices.

The exponents for the nonlinear regime predicted by both theories are very close. Simulation results could hardly discriminate between them. The main benefit of the approach presented in the appendices is conceptual. The critical shear rate turns out as the inverse of the typical residence time of a chain end in the interface (in all compression regimes). Under strong compression, as considered in our simulations, the critical shear rate also coincides with the lowest lateral relaxation frequency of a chain in the brush.

For much longer chains, each grafted chain laterally wiggles around many others. Our theory describes a nonentangled central sublayer (comprising the interface) embedded into a gel-like elastic layer. A slightly different approach is needed when the interface is wide enough to be entangled itself.

V. Comparison to Experiment and Other Numerical Approaches

Experimental limitations prevent the exploration of equivalently large compressions and shear rates as they can be studied in simulations. However, some experimental data that reach the non-Newtonian regime have become available. Schorr et al. recently measured shear forces in bilayers of polystyrene brushes on mica with the surfaces forces apparatus (SFA).[13] In toluene (good solvent), the authors observe linear response over a wide range of compressions and shear rates. However, at large compression ($2h/D \approx 4.6$)[60] they find a sublinear increase of the shear

(59) Joanny, J.-F. *Langmuir* **1992**, *8*, 989.

(60) The experiments are carried out at $D \approx D' = 95$ Å, with $h = 220$ Å the unperturbed brush height.

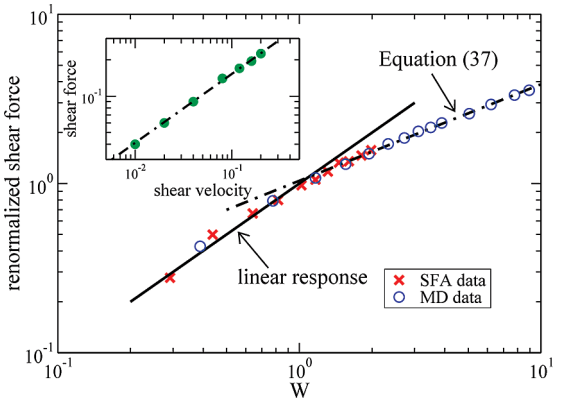

Figure 10. SFA data from PS/PVP [25/4]k in toluene at $T = 32$ °C (taken from ref 13). Shear force and velocity have been scaled by the same procedure as our simulation data [$D = 14.75$, $N = 60$, $\rho_g \approx 1.1\rho_g^*(N = 30)$, solvent-free] using $f_x(\dot{\gamma}^*) \approx 88\mu$N and $\dot{\gamma}^* \approx 16.8$/s. Both experiment and simulation find a linear increase of the shear force for $W \leq 1$ and are in agreement with eq 37 in the non-Newtonian regime. The inset shows data[13] (in LJ units) from Brownian dynamics simulations, which agree nicely with the predicted power-law of eq 37 (dash-dotted line).

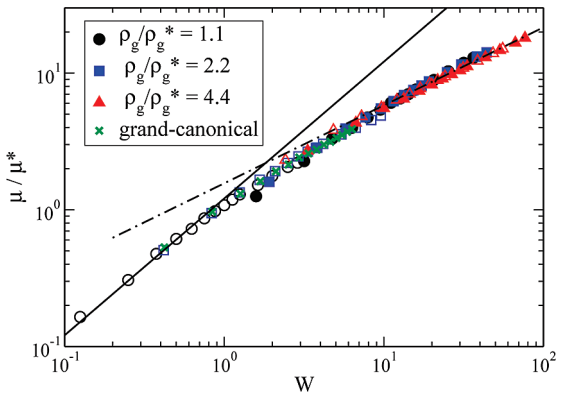

Figure 11. Renormalized kinetic friction coefficient (see text) as a function of the Weissenberg number. We show the same data as in Figure 5 but now on double−logarithmic scale. Results of grand-canonical MD simulations[61] are included. We find linear behavior (solid line) for $W \leq 1$ and a reasonable agreement to the exponent suggested by eq 37 (dash-dotted line) beyond linear response.

force with sliding velocity. Interestingly, the experimental data is comparable with eq 37 [or eq 18], as can be seen from Figure 10. Identifying the critical shear rate and $f_x(\dot{\gamma}^*)$ via the crossover from linear to non-Newtonian behavior, we can compare the SFA data to our results at similar compression and chain length. For this purpose we use a solvent-free system with $D = 14.75$, $N = 60$, and $\rho_g \approx 1.1\rho_g^* \approx (N = 30)$, corresponding to a compression of $2h/D \approx 4.1$.[37]

In the same study, Schorr et al. performed Brownian dynamics simulations using a Brinkman type equation to describe the solvent flow. They observe shear thinning at their largest compression ($2h/D \approx 7.4$) over the entire range of investigated shear rates. As shown in the inset of Figure 10, also this data follows the scaling-law predicted by eq 37, despite the different approach to treat solvent effects.

Goujon et al.[28] recently investigated sheared polymer brushes with an off-lattice bead−spring model by means of MD simulations using a DPD thermostat with larger intrinsic friction (see section II). The length of the grafted polymers ($N = 20$) was somewhat smaller than considered here.

More importantly their study differs from ours in the way solvent molecules are incorporated. While our simulations are performed at constant particle number, Goujon et al. operate in the grand-canonical ensemble, allowing the number of solvent particles to fluctuate. This procedure guarantees a constant normal pressure for all shear rates. However, our numerical data indicates that the normal stress changes very weakly with shear rate (see section IIIA).

On the other hand, a grand-canonical solvent treatment might bear the risk of suppressing some hydrodynamic correlations. Also this effect seems negligible, as can be seen from Figure 11, where we compare our data for the friction coefficient (as shown in Figure 5) to the results of Goujon.[61] Since f_z is virtually constant, the dependence of the friction coefficient and f_x on W must be similar. We find that both numerical approaches reveal the same universal behavior, which is in good agreement with eq 37. The data superimposes when the kinetic friction coefficient is normalized by $\mu^* = \mu(W = 1)$ to obtain a scaling plot.

In conclusion, we find the same universal macroscopic response in numerical simulations despite very different approaches to incorporate solvent effects, including the implicit treatment using a DPD thermostat or the self-consistent solution of the Brinkman equation. Approaches with explicit solvent molecules in different thermodynamic ensembles provide the same general picture. All these methods seem equivalently valid for steady-shear simulations of strongly compressed brushes, providing hydrodynamic correlations on the relevant length scales.

To the best of our knowledge, there is only one study[26] that reported a power-law behavior of the chain extension beyond linear response. This investigation, by one of the authors, used a Langevin thermostat without explicit solvent molecules; an approach widely used in the past (see, e.g. refs 14, 15, 19, 23, 24, 26, 27, and 30). However, the Langevin thermostat cannot account for hydrodynamic correlations, because it does not apply random and dissipative forces in a pairwise form.[62,63] In this case, the response to shear should be described by our scaling theory for semidilute, dry brushes. The previous study reported an exponent of $\phi \approx 0.6$, which is slightly smaller than our predicted value, 0.65.

VI. Summary

In the present study, we investigated polymer-brush lubrication of short chains by means of MD simulations and scaling theory. Using a classical coarse-grained polymer model, we measured the response of two opposing brush-covered surfaces to stationary Couette flows of different shear rates. We varied the compression of the confined layers and their molecular parameters, grafting density and chain length. Solvent-free systems have been compared to systems that included explicit solvent molecules (dimers).

Very different responses to shear are observed, depending on the considered parameter combinations. In particular for small grafting densities, systems with explicit solvent leave the regime of linear response earlier than their solvent-free counterparts and the kinetic friction coefficient is significantly smaller. We observe the formation of a fluid layer between the brushes for large shear rates.

The regime of linear response is left earlier with increasing compression, grafting density or chain length. In general,

(61) Goujon, F. *Dissertation*, Clermont-Ferrand, **2003**.

(62) Soddemann, T.; Dünweg, B.; Kremer, K. *Phys. Rev. E* **2003**, *68*, 046702.

(63) Langevin and DPD thermostats recently have been compared for stationary and nonstationary shear simulations of polymer brushes.[30]

non-Newtonian behavior sets in at smaller shear rates when the density of the system is increased.

In agreement with previous computer studies (see references in ref 23 and refs 24−27, 29, and 30), we observe only small changes of the layer thickness, but a pronounced swelling of polymer chains along the shear direction. This behavior goes along with a non-Newtonian response, e.g., a sublinear increase of the lateral friction force with sliding velocity.

Our data indicates that the swelling of chains in the shear direction can be described by a universal power-law increase of the chain extension (characterized by the radius of gyration) with the Weissenberg number. Using the shear-induced deformation of chains, we demonstrated how to estimate the critical shear rate. This allows one to superimpose the data of all considered parameter combinations, revealing a rather closed picture that relates the chain deformation to the macroscopic response. Despite their distinct differences, solvent and solvent-free cases can be described consistently.

We developed a scaling theory that allows one to explain the structural changes of the bilayer and its macroscopic response to shear. Our analytical approach is capable of reproducing not only the data stemming from very different numerical models but also recent experimental observations. A central result of our scaling approach is that the critical shear rate, at which the linear response regime is left and non-Newtonian behavior sets in, depends on compression and molecular parameters as

$$\dot{\gamma}^* \sim N^{-2.44} \rho_g{}^{-0.27} D^{0.6} \tag{48}$$

in the limit of strongly compressed, semidilute brushes with Zimm dynamics. Although we find a qualitative agreement between the data in Table 1 and the predicted behavior of $\dot{\gamma}^*$, the exponents suggested in eq 48 are difficult to confirm numerically. Partially, this is related to the fact that the dependence of $\dot{\gamma}^*$ on grafting density and compression is rather weak. In addition, the parameter regime that can be probed for ρ_g and D is limited because one has to ensure strongly compressed brushes. The upper limit of N, to which our theory remains valid, should be given by the entanglement length.

Our results and previous investigations[13,28] indicate that the universal macroscopic response, as we report it here for the first time, is not influenced by the way solvent effects are incorporated in detail. However, at least the structural response is altered when hydrodynamic effects are suppressed in simulations, as for instance in ref 26.

In an upcoming publication,[64] we will demonstrate that the power-law exponents obtained in this study remain unaltered, even after certain structural modifications of the explicit solvent, which is done by replacing solvent molecules with star polymers of different functionality and arm length. Future work will concern the response to nonstationary shear, such as the onset of motion, shear inversion, and oscillatory shear.

Acknowledgment. Financial support by the Agence Nationale de la Recherche (ANR-06-BLAN-0315), the ESF-STIPOMAT program, the MENESR, and the POLYMAT program (Mainz) is gratefully acknowledged. T.K. and C.P. thank the Institute of Physics at the University of Mainz for hospitality during short visits when this work was completed. We are indebted furthermore to H. Meyer, S. M. Balko, and K. Binder for carefully reading the manuscript.

(64) Spirin, L.; Galuschko, A.; Kreer, T.; Johner, A.; Baschnagel, J.; Binder, K. Manuscript in preparation.

Appendix A: Equilibrium Description

Throughout we follow the standard Milner−Witten−Cates (MWC)[54] strong stretching description (an equivalent one was developed by Zhulina and co-workers[65]). In the MWC theory, a grafted chain part of the brush with its free end located at a distance z_e from the grafting plane can be described by its optimal configuration only and other paths entering the partition sum can be discarded. This is equivalent to the classical approximation to quantum mechanics. MWC is expected to fail at the soft brush edge, a calculation taking into account fluctuations has been proposed to describe this outermost region. The main additional assumption in MWC is that the tension vanishes at the free chain ends. It follows that in this description the brush is a highly degenerate system, all end locations being equivalent. Free ends are hence expected to diffuse through the layer and exchange their positions. Simultaneously, MWC predicts a free end distribution, $g(z)$, which is not flat. As noted by several authors (see ref 66 and references therein), MWC is not strictly speaking a self-consistent (mean-field) theory.

Let us recall the brush height, h, the classical concentration profile, $\phi(Z)$, a small distance $Z \ll h$ from the edge, the correlation length in the bulk of the brush, ξ_c, and at the edge, ξ_0, according to MWC:

$$h \sim aN(\rho_g a^2)^{(1-\nu)/2\nu}, \quad \phi(Z) \sim c\left(\frac{Z}{h}\right)^{(6\nu-2)/(3-2\nu)}$$

$$\xi_c \sim a(ca^3)^{\nu/(1-3\nu)}, \quad \xi_0 \sim aN^{2\nu/3}(\rho_g a^2)^{-1/6} \tag{A1}$$

The length ξ_0 describes the soft brush edge for static properties like brush interpenetration at contact or linear dynamics like flow penetration at moderate shear rates.

When two brushes slightly overlap their interpenetration length equals ξ_0. In the opposite limit of strong compression, the concentration profile is almost flat, $\phi(z) = c \sim \rho_g N/D$. The brushes hence can be described as molten without concentration fluctuations, provided monomers are renormalized to concentration blobs of radius ξ_c and monomer content $g_c \sim (\xi_c/a)^{1/\nu}$. For a molten brush (of concentration $c \sim a^{-3}$), the classical end distribution, $g(z)$, and penetration length obey

$$g(z) \sim \frac{\rho_g z}{h\sqrt{h^2 - z^2}}, \quad \delta \sim \left(\frac{N^2 a^4}{h}\right)^{1/3} \tag{A2}$$

The end distribution is singular at the brush edge

$$g(z) \sim \rho_g \sqrt{2z/h^3}$$

but the ends are only weakly localized at the edge and remain marginally free. After renormalization to blobs we obtain

$$g(z) \sim \rho_g \sqrt{\frac{z}{D^3}}$$

$$\delta \sim a\left[N^{2\nu}(\rho_g a^2)^{2(1-2\nu)}\left(\frac{a}{D}\right)^{1-\nu}\right]^{1/3(3\nu-1)} \tag{A3}$$

Note that the edge singularity of the end distribution does not change upon renormalization to blobs. The end distribution strongly differs from the Alexander−de Gennes distribution.

(65) Zhulina, E. B.; Pryamitsyn, V. A.; Borisov, O. V. *Polym. Sci. USSR* **1989**, *31*, 205.

(66) Netz, R. R.; Schick, M. *Europhys. Lett.* **1997**, *38*, 37.

It is instructive to estimate the penetration depth δ for the upper ($D \sim h$) and lower boundary ($D \sim \delta$) of the strong compression regime. We obtain $\delta \sim a[N^{2\nu}(\rho_g a^2)^{1-3\nu}]^{1/(6\nu)}$ and $\delta \sim a[N^{\nu}(\rho_g a^2)^{1-2\nu}]^{1/(4\nu-1)}$, respectively. For $D \sim \delta$, the penetration depth merges with the isotropic chain radius at the actual brush concentration. Upon further compression the chains in the brush are not stretched but rather reflected by the surfaces, obviously the strong stretching approximation is no longer appropriate. In practice, the brush may become dense (and the equation of state assumed for the polymer solution fails) before the limit $D \sim \delta$ is reached.

At the crossover to weak compression, $D \sim h$, each chain spans the interpenetration length with $(\delta/\xi_c)^2 g_c$ monomers. Inserting values according to eqs A1 and A3 we find $(\delta/\xi_c)^2 g_c \sim g_0$, i.e. the same number as for brushes that are just in contact. We may conclude that the number of monomers per chain in the interpenetration layer is almost constant over the whole weak interpenetration regime. Thus, the weak compression regime ($d = 2h - D \ll h$) is characterized by the correlation length

$$\xi_d \sim \xi_c \left(\frac{d}{h}\right)^{2\nu/(2-3\nu)} \tag{A4}$$

and the interpenetration depth

$$\delta \sim \left(\frac{g_0}{g_c}\right)^{1/2} \xi_c \sim \xi_0 \left(\frac{d}{\xi_0}\right)^{(1-2\nu)/(3-2\nu)} \tag{A5}$$

Inserting $\nu \approx 0.588$, the interpenetration is found to slightly decrease upon weak compression.

Appendix B: Linear Shear Regime

The linear shear regime is tightly linked to the previous section as by definition the brush structure is only slightly disturbed and hence is assumed to be preserved to leading order. It is convenient to start out from the case of a single brush sheared through a solvent layer. This case was thoroughly analyzed in ref 58. The penetration depth of the flow into the brush is ξ_0. Assuming that the same chains stay in the sheared edge all the time and sustain the hydrodynamic force, f, we could naively apply the fluctuation dissipation theorem and calculate the mean lateral deflection, $R_x = f\langle R_x^2\rangle$ ($k_B T \equiv 1$). This is not justified as chain ends exchange their position over time. Rather, a given end typically leaves the sheared layer after the relaxation time associated with ξ_0, $\tau_0 \sim \eta_s \xi_0^3$. The actual deflection of a chain end depends on its history, more precisely on the previous visits to the sheared layer. Obviously, visits done more than one lateral relaxation time ago do not matter. On the other hand, the response function to the localized shear force only decays as a weak power of time.[58] What finally matters is the average hydrodynamic force exerted on the end about one lateral relaxation time ago. An end currently located in the sheared layer is likely to be most deflected (as compared to those found deeper in the brush). One lateral relaxation time ago its probability density was spread over one isotropic radius in depth. Hence, the average force can be estimated as

$$\langle f \rangle \approx f\xi_0/\sqrt{\langle R_x^2\rangle}$$

yielding

$$\frac{R_x}{\sqrt{\langle R_x^2\rangle}} \sim f\xi_0 \sim \eta_s \xi_0^3 \dot{\gamma} \tag{B1}$$

when we insert the hydrodynamic force, $f \sim \eta_s \xi_0^2 \dot{\gamma}$, exerted on one end within the sheared layer. The threshold to non-Newtonian behavior corresponds to a deflection as large as the thermodynamic fluctuation, hence the critical shear rate corresponds to the relaxation frequency of the last blob, $\dot{\gamma}^* \sim 1/\eta_s \xi_0^3$.

The case of two brushes in contact sheared against each other should be very similar. Formally, there are two sources of dissipation, the drag of the polymers and the shear flow imposed to the solvent in the interface. Both give contributions scaling as $\eta_s \dot{\gamma} h \xi_0$. The drag is that of a blob through a mesh of width similar to its own size, which only marginally differs from the drag through solvent. The dissipation in the shear flow corresponds to the effective velocity drop, $\dot{\gamma}h$, through the interfacial layer of thickness ξ_0. Taking into account chain-end exchange yields

$$\frac{R_x}{\sqrt{\langle R_x^2\rangle}} \sim \eta_s \xi_0^3 \frac{h}{\xi_0} \dot{\gamma} \tag{B2}$$

This result is identical to eq B1 if we replace $\dot{\gamma}$ by the effective shear rate in the interface, $\dot{\gamma} D/\xi_0$.

In the weak compression regime, the drag force on a chain moving in the interface of thickness δ reads $f \sim \eta_s (\delta/\xi_d)^2 \xi_d \dot{\gamma} D$. Chain-end exchange reduces the force by a factor of

$$\delta/\sqrt{\langle R_x^2\rangle}$$

Collecting all factors we obtain a result very similar to eq B2

$$\frac{R_x}{\sqrt{\langle R_x^2\rangle}} \sim \eta_s \frac{\delta^4 D}{\xi_d \delta} \dot{\gamma} \tag{B3}$$

In analogy to the case of brushes at contact, the relaxation time, $\eta_s \delta^4/\xi_d$, of a section spanning the interface is multiplied by the effective shear rate in the interface.

In the strong compression regime, eq B3 remains valid provided ξ_d is replaced by ξ_c. It is nonetheless instructive to recast this formula into the equivalent form,

$$\frac{R_x}{\sqrt{\langle R_x^2\rangle}} \sim \eta_s \left(\frac{N}{g_c}\right)^2 \xi_c^3 \dot{\gamma} \tag{B4}$$

showing that the critical shear rate can be understood as the lateral Rouse/Zimm relaxation frequency of a chain in the brush. Inserting the expression for ξ_c with $c \sim N \rho_g/D$ finally gives

$$\dot{\gamma}^* \sim \frac{1}{\eta_s a^3}\left[N^{-3\nu}\left(\frac{\rho_g a^3}{D}\right)^{3\nu-2}\right]^{1/(3\nu-1)} \tag{B5}$$

or, with $\nu \approx 0.588$

$$\dot{\gamma}^* \sim N^{-2.31}\left(\frac{D}{\rho_g}\right)^{0.31} \tag{B6}$$

The scaling with N and ρ_g is very similar compared to the model presented in the main text. Only the dependence on D differs drastically. A critical test to distingiush between the suggested exponents remains difficult, as already mentioned. In the Rouse regime of dry, dense (nonswollen) brushes, we obtain

$$\dot{\gamma}^* \sim \frac{1}{\psi(Na)^2} \tag{B7}$$